



Critical role of sodium migration in iron-based FT- zeolite tandem catalyst system for syngas hydrogenation to gasoline

Ruifeng Wang^{a,b,c}, Binglian Liang^a, Xiaoli Yang^a, Xuning Li^a, Yaru Zhang^{a,b}, Guodong Liu^a, Xiong Su^{a,*}, Yanqiang Huang^{a,*}, Tao Zhang^{a,b}

^a State Key Laboratory of Catalysis, Dalian Institute of Chemical Physics, Chinese Academy of Sciences, No. 457 Zhongshan Road, Dalian 116023, China

^b University of Chinese Academy of Sciences, Beijing 100049, China

^c Zhang Dayu School of Chemistry, Dalian University of Technology, Dalian 116024, China

ARTICLE INFO

Keywords:

Syngas
FTO-ZEO
Fischer-Tropsch synthesis
Zeolites
Na promoter

ABSTRACT

Exploration the role of promoter in the Fischer-Tropsch zeolite (FTO-ZEO) tandem catalyst systems is of paramount importance in improving the selectivity of target products. Herein, by varying the contents of Na promoter in $x\text{Na-FeO}_x$, the evolution of Na in FTO-ZEO system during reaction and the resultant catalytic performance for FT synthesis have been investigated. When the content of Na falls in the range of 0.5–5 %, the syngas conversion performance on bare FeO_x catalysts reaches a performance-platform period, while that on tandem catalysts show a volcano-like trend. With a set of control experiments, it is speculated that there is a migration process of Na from $x\text{Na-FeO}_x$ to the H-ZSM-5 moiety. The changed acidity of H-ZSM-5 causes the transformation of products toward higher carbon alkanes and aromatics in the gasoline range with a selectivity of 71.5 %. This work makes an important progress by showing the phenomenon of Na migration during reaction, which puts forward the influence of promoters on FTO-ZEO system and gives a new insight of zeolites modification.

1. Introduction

With the increasing shortage crisis of petroleum resources, liquid fuels based on petroleum refining is in urgent need of alternative routes [1–4]. The transformation of syngas, a mixture gas of CO and H_2 often obtained from coal, biomass, natural gas or carbon dioxide, into high value-added products (also known as Fischer-Tropsch synthesis) has become the most promising path [5–8]. For Fischer-Tropsch (F-T) synthesis, Fe, Co, Ru-based catalysts have been widely investigated [6,9,10], among which iron-based catalysts have drawn considerable attention due to their low harmfulness, low cost, flexible operation conditions and high selectivity toward olefins [11–13]. However, the product selectivity of F-T synthesis obeys the Anderson-Schulz-Flory (ASF) distribution rule, which will lead to a considerable yield of non-target products [14,15]. In recent years, the combination of oxide-zeolite (OX-ZEO) system, which employs tandem catalysts containing oxides and zeolites, breaks the ASF distribution and may gain higher selectivity toward target products [16,17]. Similarly, the system of FTO-ZEO, which employs tandem catalysts containing Fe-based F-T catalysts and

zeolites, has also been researched extensively [18–25]. For instance, Zhao et al. [18] adopted a combination of Fe-based catalysts and hierarchical HZSM-5 with uniform mesopores, which effectively broke the ASF distribution. During the stable stage, the selectivity of aromatics achieved about 51 % with the conversion of CO higher than 85 %. Similarly, the well-designed core-shell structure with Fe_3O_4 @ MnO_2 and hollow HZSM-5 construction exhibited excellent F-T performance, with the selectivity of aromatic reached to 57 % at CO conversion of 90 % [25]. Compared with OX-ZEO, the FTO-ZEO system shows higher CO conversion, higher target product yield and flexible reaction conditions. Thus, it is worth great prospects for further research.

Normally, the introduction of promoters to the component of oxide or FT synthesis catalyst has also been demonstrated an efficient way to improve the selectivity of target product [26]. Among various promoters, alkali metals are normally added to iron-based catalysts [27–32]. Li et al. [27] found that alkalis could form a strong interaction with iron species during the reduction of catalysts. Moreover, the carbonization of catalysts, during which the formation of iron carbide active center for FT synthesis, can be facilitated by alkalis. As reported

* Corresponding authors.

E-mail addresses: suxiong@dicp.ac.cn (X. Su), yqhuang@dicp.ac.cn (Y. Huang).

<https://doi.org/10.1016/j.apcatb.2022.122132>

Received 5 September 2022; Received in revised form 24 October 2022; Accepted 28 October 2022

Available online 31 October 2022

0926-3373/© 2022 Elsevier B.V. All rights reserved.

by Xiong et al. recently [30], with the increase of atomic number of alkalis, the influence of alkalis to the FT synthesis performance increases.

In this condition, to obtain higher selectivity of target product, the combination of FTO-ZEO system and the introduction of alkali metals to Fe-based catalysts might be one of the most effective way [18,20]. The effect of alkali promoter on the Fe-based catalyst can be predicted by illustrating the structure of iron component. Nevertheless, the influence of promoter on the other semi-component and the resultant catalytic performance in FTO-ZEO system is often overlooked. Especially, highly-active promoters (e.g. Na) initially added in the ferric oxide component, may migrate to zeolite to form a more efficient status as the evolution of reaction. The process of element migration and the role toward catalytic performance in composite catalysts has been discussed recently [33–35]. For instance, Wang et al. investigated the CO₂ hydrogenation reaction with the combination of a representative oxide and zeolites [33], in which they found that the protonic sites of zeolites have been neutralized by a strong thermomigration of metal, resulting in a decrease in the selectivity of C₂₊ products. Identically, the effect of element migration has also been excavated in a FTO-ZEO system [34], during which Na⁺ migration played a critical role in suppressing H-transfer. The change in small amount of Na⁺ migration can help gain more light α -olefins. Despite these primary studies, detailed research works on the effect of promoters, as a migration process during the evolution of reaction, may provide more insights in this important tandem catalytic system.

Herein, the FTO-ZEO system has been constructed by tandem catalysts containing xNa-FeO_x and H-ZSM-5. We investigate the influence of Na on the two active species in this system by changing the amount of Na on the iron-based catalyst. The migration of Na promoter from ferric oxide component to zeolite has been discovered and deeply investigated. Also, the reaction performance and targeted characterizations of iron-based catalyst and the tandem catalytic system during the evolution stage have been tested, which can help explain the improvement for the conversion of syngas into gasoline products on this catalytic system.

2. Experimental section

2.1. Catalyst preparation

2.1.1. Synthesis of xNa-FeO_x catalyst

A series of xNa-FeO_x catalysts were prepared by an incipient wetness impregnation method. Typically, a certain amount of NaNO₃ (Aladdin, 99 % AR grade) was dissolved evenly into 1.74 g deionized water. Then, 3 g of Fe₃O₄ powder (Aladdin, 99 % AR grade) was added to the former sodium nitrate solution, which was followed by stirring and ultrasonic treatment. The obtained slurry was aged at 25 °C for 12 h and then dried in a vacuum oven at 60 °C for 12 h. The resultant sample was placed into a muffle furnace and heated to 400 °C at a heating rate of 5 °C min⁻¹ and kept for another 3 h. To examine the effect of Na promoter, a series of xNa-FeO_x samples (x denotes the mass content (wt%) of Na promoter to the Fe-based catalysts) were prepared according to the same procedures.

2.1.2. Synthesis of H-ZSM-5 catalyst

H-ZSM-5 catalyst was prepared by a hydrothermal synthesis method. In a typical preparation process, 0.6 g Al(NO₃)₃·9H₂O, 26.2 g tetrapropyl ammonium hydroxide (TPAOH), 22.4 g tetraethoxysilane (TEOS), 0.2 g NaOH, 0.2 g isopropanol and 4.0 g urea were dissolved in sequence into 36.8 ml deionized water with vigorous stirring for 2 h. After a thorough mixing, the obtained slurry was transferred into a steel autoclave with PTFE lining, sealed, and crystallized at 180 °C for 48 h. The as-obtained precipitate was filtered and washed with deionized water for several times. The resultant sample was dried at 100 °C overnight, and calcined at 550 °C in a muffle furnace for 5 h. Before obtaining the final H-ZSM-5 catalyst, ammonia exchange, phosphorus modification and hydrothermal treatment procedures were conducted. A hydrothermal treatment at 550 °C was proceeded with the aim of

removing strong acid sites. Typically, 10 g H-ZSM-5 was put into a tubular furnace and heated to 550 °C. Then, the tubular furnace was pumped with water (10 ml min⁻¹), filled with water vapor and kept at 550 °C for 1 h. Phosphorus modification was conducted by impregnating H-ZSM-5 with Ammonium dihydrogen phosphate. For a typical phosphorus modification treatment, 0.148 g ammonium dihydrogen phosphate was dissolved evenly into 1.8 g deionized water. Then, 2 g of H-ZSM-5 was added into the solution, followed by stirring and ultrasonic treatment. The obtained slurry was aged at 25 °C for 12 h and then dried in a vacuum oven at 60 °C for 12 h. The resultant sample was placed into a muffle furnace and heated to 550 °C at a heating rate of 5 °C min⁻¹ and kept for 3 h. Besides, 0.2Na-im-H-ZSM-5, which indicates Na impregnated H-ZSM-5 by direct impregnation, was also prepared by an incipient wetness impregnation method. Except for a difference of the calcination treatment at 400 °C for 3 h, the other preparation conditions are the same as phosphorus modification of zeolite. After these pretreatment procedures, both xNa-FeO_x and H-ZSM-5 were compressed and crashed into small pellets (40–60 mesh) for further catalytic tests.

2.2. Activity measurements

Before conducting CO hydrogenation tests, xNa-FeO_x and H-ZSM-5 were mixed evenly in a certain proportion. To control variables, xNa-FeO_x catalysts were tested individually, which were mixed with quartz sand (40–60 mesh) to exclude other influences. Normally, 0.3 g sample (xNa-FeO_x: H-ZSM-5 or quartz sand = 1: 5 in mass) was stacked in a fixed-bed stainless steel reactor (i.d. of 8 mm). Firstly, the sample was reduced in H₂ atmosphere (0.1 MPa with a flowrate of 30 ml min⁻¹) at 350 °C for 5 h. When the temperature dropped below 280 °C, the gas flow was switched to syngas (H₂: CO: Ar = 64 %: 32%: 4 %) for further test. The catalytic performance test was conducted under a condition of 320 °C, 3 MPa, with a gas hourly space velocity (GHSV) of 6000 h⁻¹ unless otherwise explained. The measurement condition was the most suitable status by doing control experiments (Fig. S1). The catalytic performance data were collected after the reaction was kept stable for 20 h. After testing, the gas was switched to Ar flow (30 ml min⁻¹) immediately for 5 h to remove hydrocarbons and carbon deposits on the catalyst surface. After filtered through a heat trap, full component products were analyzed by an online gas chromatographs (Agilent 7890B), which were equipped with a flame ionization detector (FID) and a PONA capillary column to analyze hydrocarbons. After that, the products were separated by a cold trap (The temperature is 0 °C) to withhold water and liquid products, which were further analyzed by GC-MS. The remaining products were transported into another online gas chromatograph (Agilent 7890B) equipped with a thermal conductivity detector (TCD) and a packed column (TDX-01) to analyze Ar, CO, CO₂, CH₄, C₂H₄ and C₂H₆. For analysis, CH₄ was taken as a reference bridge between TCD and FID. An internal standard curve method by using Ar as the internal standard substance was considered for the quantitative calculation. The specific formulas are given in the following:

$$X_{CO} = \frac{n_{in}(CO) - n_{out}(CO)}{n_{in}(CO)} = 1 - \frac{A_{out}(CO)/A_{out}(Ar)}{A_{in}(CO)/A_{in}(Ar)} \quad (1-1)$$

where, X_{CO} refers to CO conversion. $N_{in}(CO)$ and $n_{out}(CO)$ mean the CO mole number of inlet and outlet; $A_{in}(CO)$, $A_{out}(CO)$, $A_{in}(Ar)$ and $A_{out}(Ar)$ mean the CO and Ar peak areas of inlet and outlet, respectively.

$$S_{CH_4} = \frac{n_{out}(CH_4)}{n_{in}(CO) - n_{out}(CO)} = \frac{f_{CH_4/Ar}[A_{out}(CH_4)/A_{out}(Ar)]}{f_{CO/Ar}[A_{in}(CO)/A_{in}(Ar) - A_{out}(CO)/A_{out}(Ar)]} \quad (1-2)$$

Where, S_{CH_4} refers to the selectivity of CH₄. $N_{out}(CH_4)$ refers to the mole number of CH₄ at outlet. $A_{out}(CH_4)$ refers to the peak area of CH₄ at outlet. $f_{CH_4/Ar}$ and $f_{CO/Ar}$ refer to the relative correction factors of CH₄ and CO to Ar. Similarly, S_{CO_2} was obtained by the same formula.

$$S_{C_xH_y} = \frac{x n_{out}(C_xH_y)}{n_{in}(CO) - n_{out}(CO)} = \frac{x f_{C_xH_y/CH_4} A_{out}(C_xH_y)}{A_{out}(CH_4)} S_{CH_4} \quad (1-3)$$

Where, $S_{C_xH_y}$ refers to the selectivity of C_xH_y . $N_{out}(C_xH_y)$ refers to the mole number of C_xH_y at outlet. $A_{out}(C_xH_y)$ and $A_{out}(CH_4)$ refer to the peak areas of C_xH_y and CH_4 at outlet.

Based on full component analysis, which indicates the selectivity of C_xH_y by FID, we obtained the carbon balance in a range of 98–102 %. Therefore, the selectivity of C_{5+} was calculated by the following formula:

$$S_{C_{5+}} = 1 - S_{CH_4} - S_{C_2} - S_{C_3} - S_{C_4} \quad (1-4)$$

Unless otherwise specified, the selectivities of CH_4 , C_xH_y and C_{5+} were determined with the removal of CO_2 .

2.3. Catalyst characterizations

For a comparable study of the change-of-state of catalysts during the catalytic process, both fresh and spent catalysts were considered for sufficient characterizations. The spent physically mixed catalyst pellets after reaction were separated by a magnetic separation. The spent H-ZSM-5 catalysts were denoted as xNa-H-ZSM-5, corresponding to their utilization with the series of xNa-FeO_x catalysts.

X-ray diffraction (XRD) experiments were tested on a PANalytical X'Pert-Pro powder X-ray diffractometer equipment with a Cu K α monochromatized radiation detector ($\lambda = 0.1541$ nm, 40 mA, 40 kV). The instrument was operated in the 2θ range of 10–90°. N₂-physical adsorption measurements were conducted on an ASAP 2010 Micromeritics instrument to obtain the specific surface area and pore volume parameters. Before analyzing, the samples were vacuumized at 350 °C for 5 h. The element contents were measured on an inductively coupled plasma optical emission spectrometer XSP instrument (ICP-OES, IRIS Intrepid II). X-ray photoelectron spectroscopy (XPS) tests were conducted on a Thermofisher ESCALAB 250Xi spectrometer, which used Al K α ($h\nu = 1486.6$ eV) as the X-ray source with a pass energy of 20 eV. Transmission electron microscope (TEM) photographs and the energy-dispersive X-ray spectroscopy (EDS) were obtained on a JEOL JEM-2100 instrument at 200 kV.

NH₃ temperature programmed desorption experiments (NH₃-TPD) were investigated on a Micromeritics AutoChem II 2920 chemisorber. Firstly, the sample in a U tube was pretreated at 450 °C for 30 min and cooled down to 50 °C under He atmosphere. A NH₃ flow was allowed to pass through the catalyst in the U tube until the sample reached saturated adsorption. Afterwards, the gas flow was switched to He and heated to 800 °C with a heating rate of 10 °C min⁻¹. The signal of NH₃ desorption was recorded on a mass spectrometer equipment.

The room temperature ⁵⁷Fe Mössbauer spectrum was observed on a Topologic 500A spectrometer, which equipped ⁵⁷Co(Rh) as the radioactive source. Fitted by the MössWinn 4, all of the spectra were distinguished by different parameters, such as quadrupole splitting (QS) and isomer shift (IS). Besides, an α -iron foil was used to calibrate the IS values and Doppler velocities.

Pyridine adsorption infrared spectroscopy (Py-IR) was characterized with a BRUKER Equinox 55 spectrometer, by using a transmission mode and a resolution of 4 cm⁻¹ in the range of 4000–400 cm⁻¹. After the pretreated process of the sample wafers at 450 °C for 30 min in dynamic vacuum, the pyridine vapor was introduced into the cell and kept for 5 min until the samples reached saturated adsorption. After the samples cooled down to 50 °C and were evacuated at 150 °C, IR spectra were collected. The quantities of Brønsted (B) and Lewis (L) acid sites were estimated based on the integrated IR peak areas at the bands of 1540 and 1450 cm⁻¹, respectively.

3. Results and discussion

3.1. Reaction performance over Na-promoted Fe-based catalysts and the tandem catalyst systems

We firstly investigated the performance of Na-promoted Fe-based catalysts, as displayed in Fig. 1A and Table S1. The series of xNa-FeO_x catalysts show excellent F-T catalytic performance, which maintain both high CO conversion and product (C_{5+} and olefin) selectivities. On bare FeO_x catalyst, CO conversion reaches to 83.1 %; however, low carbon alkanes (C_{1-4}) are the main products. Obviously, the introduction of a small amount of Na, for instance 0.2 %, affects the iron-based catalyst and changes the reaction performance. With the content of Na increasing, the selectivity of C_{1-4} alkanes decreases distinctly, while the selectivities toward C_{2-4} olefins and C_{5+} hydrocarbons increase. It is noteworthy that when the content of Na is more than 0.5 %, the performance, especially the product selectivity over Fe-based catalysts varies slightly. This result is almost consistent with our previous work [36]. For further discussion, we define the stage of Na content ranging from 0.5 % to 5 % as a performance-platform period.

As referred to CO conversion, when the content of Na is low, the bare FeO_x and 0.2Na-FeO_x catalysts show excellent conversion up to 83 %. However, if the contents of Na are higher than 0.5 %, the catalysts show activity decay from 83 % to nearly 50 %. It has been suggested that, with the addition of Na promotor to iron-based FT synthesis catalysts, the production of heavy components such as C_{5+} increases. C_{5+} attaches to and may cover the active sites, resulting in the reduction of the conversion [27,37].

Further, the tandem catalysts containing Na-promoted-Fe-based catalysts and H-ZSM-5 have been explored (see Fig. 1B and Table S2). The tandem catalysts which use the same H-ZSM-5 zeolite with a hierarchical pore structure (Fig. S2) perform a lower selectivity of C_{2-4} olefins but a higher selectivity toward C_{5+} hydrocarbons compared with their corresponding Fe-based counterparts. We speculate that the introduction of H-ZSM-5 promotes the oligomerization and aromatization of C_{2-4} olefins, which can be also verified from other works [8,18]. The transformation of olefin to higher carbon products can also drive the dynamic conversion of CO up to about 90 %. For all these catalyst systems, the conversion remains almost stable irrespective of the Na contents. It can be explained as that the intermediate products are transferred by H-ZSM-5 in time, which makes the conversion maintain at high levels. Besides, with the increase of Na content over these tandem catalysts, the selectivities of CH_4 and C_{2-4} alkanes decrease while that of C_{2-4} olefins increases slightly. There is another interesting finding that the selectivity of C_{5+} shows a volcanic-like trend over these tandem catalysts. With 2.5 % of Na loading, the tandem catalyst shows the best performance with the CO conversion and C_{5+} selectivity reach up to 91.6 % and 71.5 %, respectively.

On the basis of these results, we conclude that the introduction of Na promotor distinctly affects the catalytic performance in both Fe-based catalysts and tandem catalysts. In the range of 0.5–5 % Na, the performance of Na-promoted Fe-based catalysts is almost stable, which is denoted as a performance-platform period. However, the tandem catalysts, which contain the same H-ZSM-5 and Fe-based catalysts with different Na contents show a volcanic-like trend in the selectivity of C_{5+} . The above phenomena give us an intuitive evidence that Na promotor has a certain influence on the H-ZSM-5 semi-component despite it was only loaded on the iron-based catalyst initially. Thus, further research will be focused on the catalyst structure and the performance changes during this platform period.

3.2. Catalyst characterization

3.2.1. The characterization of Fe-based catalysts

We firstly focus on the structures of both fresh and spent Fe-based catalysts with different contents of Na, which are separated from

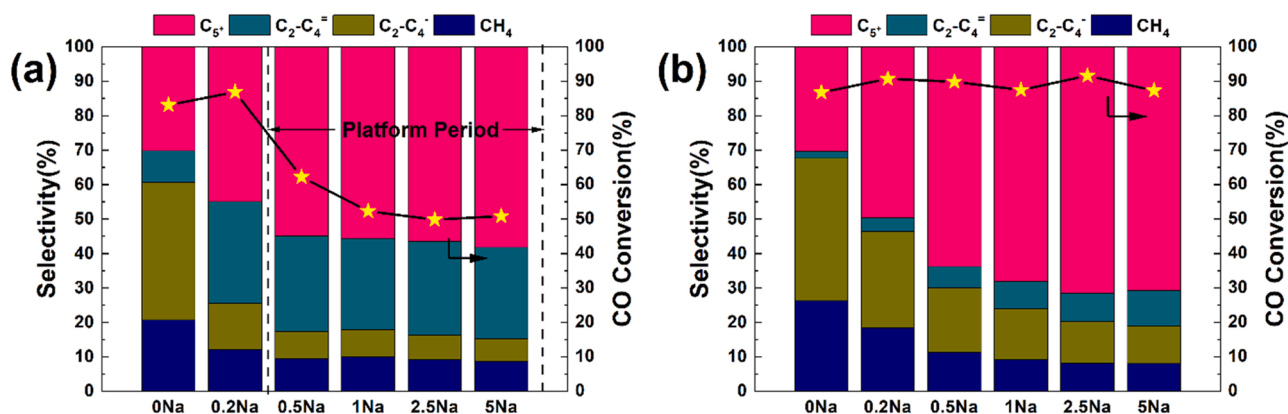


Fig. 1. The reaction performance of (a) Na-promoted Fe-based catalysts and (b) xNa-FeO_x and H-ZSM-5 tandem catalysts for syngas hydrogenation. Reaction conditions: 320 °C, 3 MPa, 6000 ml g_{cat}⁻¹ h⁻¹, H₂/CO = 2. The mass ratio of Fe-based catalysts/ zeolite = 1: 5.

tandem catalysts. Fig. 2A shows the XRD patterns of the series fresh xNa-FeO_x catalysts. The peaks at 30.24°, 35.63° and 62.93° are indicative of the existence of γ-Fe₂O₃ (PDF card no. 39-1346). Besides, the diffraction peaks at 33.17°, 35.63°, 54.08°, 62.45° and 64.02° are assigned to α-Fe₂O₃ (PDF card no. 79-1741). A weak signal at 29.45° is attributed to NaNO₃ (PDF card no. 07-0271). It is suggested that excessive addition of Na will form a crystal phase of NaNO₃, which is not conducive to the dispersion of Na. Besides, with the increase of Na content, the phase of iron species has changed from α-Fe₂O₃ to γ-Fe₂O₃. These findings lead us to conclude that the loading of Na on the Fe-based catalysts causes an obvious change in the iron phase before reaction. In Fig. 2B, the XRD patterns of spent Fe-based catalysts have been observed. Irrespective of Na contents, the iron species in all these samples presents an iron carbide phase. Compared with the bare FeO_x catalyst, the addition of Na facilitates the formation of iron carbide, as indicated by the relative intense signals.

Based on XRD characterization, the structure differences of iron carbide between these catalysts are still difficult to be distinguished, which deserves further analyzes. Mössbauer spectroscopy has been considered as an effective technology to quantitatively distinguish the phase and content of iron carbide species. The Fe-based catalysts separated from tandem catalysts has been tested by Mössbauer spectroscopy (Fig. 3). We chose both fresh and spent xNa-FeO_x (x = 0.5 and 2.5) catalysts for a comparative study. In the spectra, the sextet with isomer shift (IS) of 0.37 mm s⁻¹ and magnetic hyperfine fields of 515.7 kOe can be assigned to hematite (α-Fe₂O₃) with large particle size, while the sextet with IS of 0.32 mm s⁻¹ and magnetic hyperfine fields of 499.6 kOe can be ascribed to Maghemite (γ-Fe₂O₃) in small particles [38,39].

Similar parameters are applied in the 2.5Na-FeO_x catalyst (Table S3). As shown, the contents of α-Fe₂O₃ and γ-Fe₂O₃ in fresh 2.5Na-FeO_x are close to that in fresh 0.5Na-FeO_x. From this data, we can conclude that in the platform period the introduction of Na has little effect on the phase of iron species, corresponding to the XRD results.

The Mössbauer spectra of spent Fe-based catalysts separated from tandem catalysts have also been measured. As shown in Figs. 3C, 3D and Table S3, the two spent Fe-based catalysts of 0.5Na-FeO_x and 2.5Na-FeO_x show co-existence of minor Fe₃C and major γ-Fe₅C₂. In detail, three sextets with magnetic hyperfine fields of 181.1, 108.9 and 219.7 kOe can be assigned to γ-Fe₅C₂, while another sextet signal at 195.8 kOe can be ascribed to Fe₃C [34,40–44]. Comparatively, the contents of Fe₃C and γ-Fe₅C₂ are almost identical. Therefore, in the platform period, Na promotor also has little impact on the phase of iron species in spent catalysts.

In combination with XRD and Mössbauer results, we can find that during the platform period, Na promotor has little effect on the phase of iron species in iron-based catalysts neither before nor after. Therefore, factors that may affect the performance of tandem catalysts are focused on the effect of Na on H-ZSM-5.

3.2.2. The characterization of H-ZSM-5

To explore the effect of Na on H-ZSM-5, the basic physical properties of fresh and spent H-ZSM-5 were investigated. The XRD patterns have been observed and shown in Fig. S2A. The peaks at 7.97°, 8.82°, 8.92°, 23.08° and 23.32° show characteristics of ZSM-5 structure. It is found that the peak positions of all samples do not change, indicating Na promotor does not affect the crystal structure of H-ZSM-5. Meanwhile,

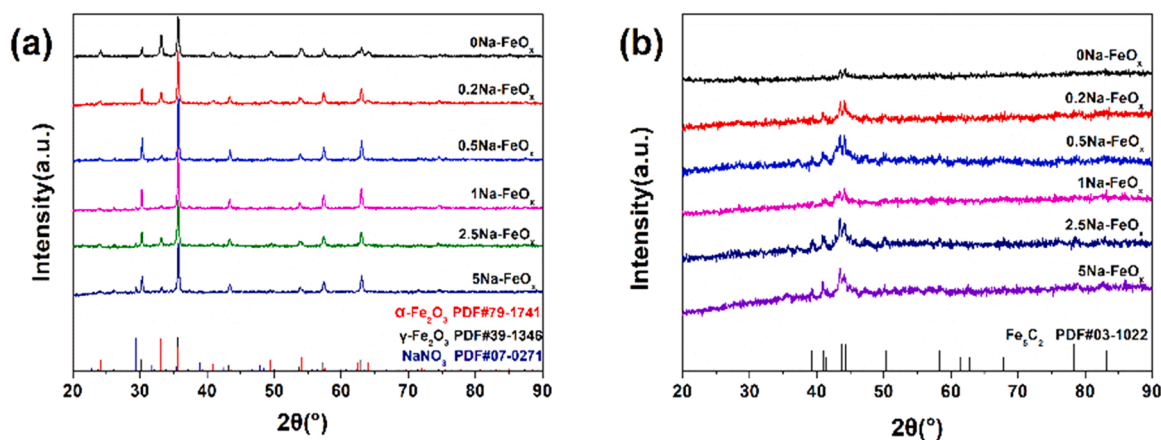


Fig. 2. XRD patterns of xNa-FeO_x collected from tandem catalysts (a) before and (b) after reaction. xNa-H-ZSM-5 means H-ZSM-5 after being used with xNa-FeO_x in syngas hydrogenation reactions.

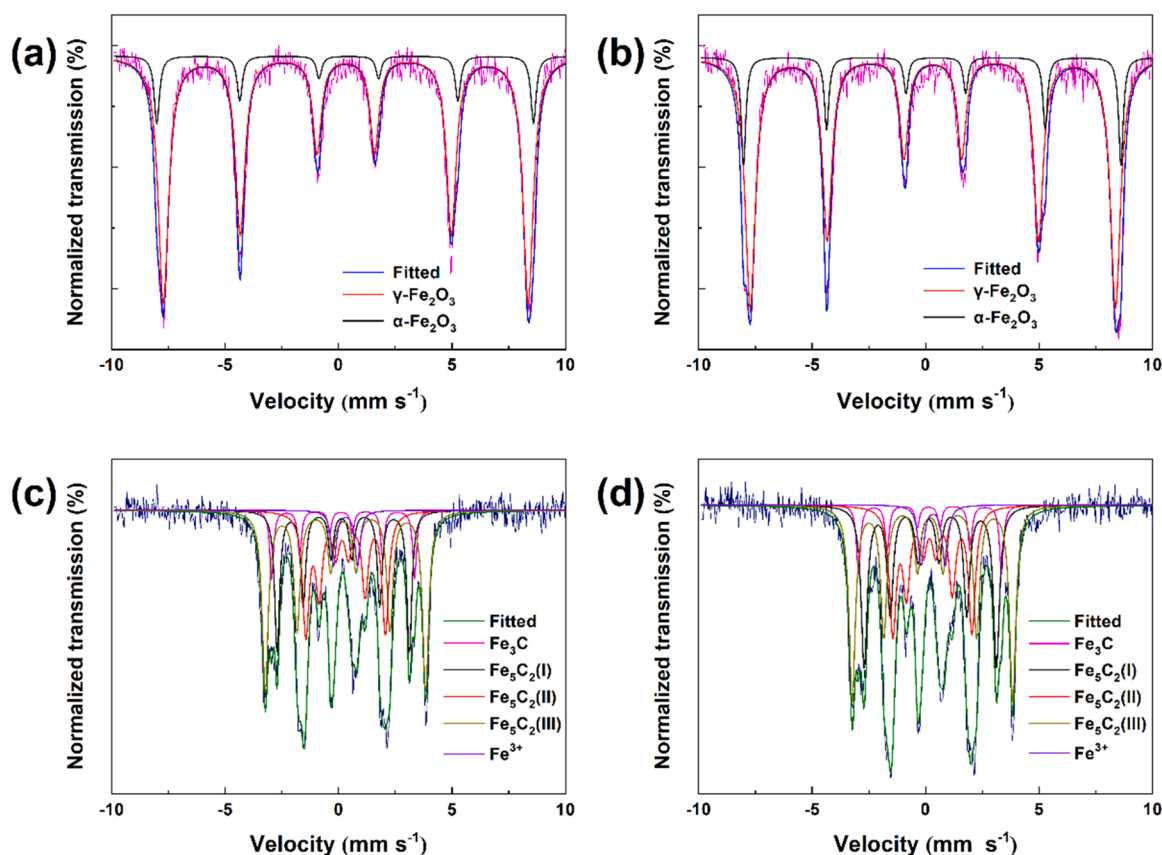


Fig. 3. Mössbauer spectroscopies of (a) 0.5Na-FeO_x and (b) 2.5Na-FeO_x before reaction; (c) 0.5Na-FeO_x and (d) 2.5Na-FeO_x after reaction.

the peak intensity of all spent H-ZSM-5 is weaker than that of fresh H-ZSM-5.

N₂ physical adsorption-desorption has been tested to further explore the texture properties of H-ZSM-5. In Fig. S2B, the isotherms show typical type IV curves. The specific surface areas of H-ZSM-5 measured by Brunauer-Emmett-Teller (BET) equation can be determined. The 0Na-H-ZSM-5 catalyst, without the addition of Na to FeO_x, owns the biggest specific surface area of 281.0 m² g⁻¹. The specific surface areas of 0.2Na-H-ZSM-5, 1Na-H-ZSM-5, and 2.5Na-H-ZSM-5 are 238.7, 207.2, and 243.2 m² g⁻¹, respectively, suggesting that the introduction of Na affects the physical properties of H-ZSM-5 after reaction. This conclusion can also be verified by the declined value of total pore volume (Table S4). Combined with XRD and N₂ physical adsorption-desorption, we speculate that the content of Na loaded on Fe-based catalysts has a negligible effect on physical properties of spent H-ZSM-5 during the platform period.

To further clarify the influence of Na on H-ZSM-5, the acidic properties of spent H-ZSM-5 have been explored. The amount of acid has been determined by NH₃-TPD technique, see Fig. 4A. In all patterns, there are two main peaks which are attributable to the weak acid at 190 °C and the strong acid at 340 °C. Due to H-ZSM-5 has been treated with water vapor and modified by phosphoric acid, the original amount of strong acid is quite low. Thus, the acid amounts of spent H-ZSM-5 are represented by total acid sites. As shown in Fig. 4B, with the Na contents on the iron-based catalyst increasing, the amounts of total acid sites in H-ZSM-5 present an inverted volcano-like trend in the platform period. The acid site amounts vary from 20.0 μmol g⁻¹ on 0.5Na-H-ZSM-5–15.7 μmol g⁻¹ on 2.5Na-H-ZSM-5, and increase slightly to 16.9 μmol g⁻¹ on 5Na-H-ZSM-5. This result evidenced that the acidic properties of H-ZSM-5 should be affected by the different Na contents even if it is only incorporated in the iron-based catalysts. Besides, the key point of the above phenomenon is that the amount of acid site of

spent H-ZSM-5 shows a relevant relationship with the C₅₊ selectivity. Regarding the volcano-like distribution of zeolite acidity, it is suspected that excessive Na doping leads to the formation of NaNO₃, which is not conducive to the migration of Na, but making the acidity rise at 5Na-H-ZSM-5.

Py-IR spectra were collected to further check the variation in the number of B and L acid sites (see Fig. 4C, D). The peaks at 1540 and 1450 cm⁻¹ can be attributed to B and L acid sites, respectively. We quantitatively calculated the amounts of the two acid sites on spent H-ZSM-5, as shown in Fig. 4D. In the performance-platform period, the amounts of both B acid and L acid sites in H-ZSM-5 also present an inverted volcano-like trend, in accordance with the phenomenon from NH₃-TPD characterization. From NH₃-TPD and Py-IR spectra, we speculate that Na species loaded on iron-based catalyst affects the acidity of H-ZSM-5 as the evolution of FT reaction, which further affects the catalysts performance [34,35].

For exploring the way that how Na affects the acidity of spent H-ZSM-5, characterizations, such as ICP, XPS, and TEM techniques, have been carried out. The element contents of spent xNa-H-ZSM-5 were determined by ICP-OES, as shown in Table 1. Both Na and Fe elements have been found on the spent H-ZSM-5 zeolites. With the increase of Na contents on iron-based catalysts, the Na content on the spent H-ZSM-5 also increases. The variation in the contents of Na on H-ZSM-5 is consistent with their character of acidity properties. On the contrary, Fe elements on the spent H-ZSM-5 show a decreased tendency. As such, the Na/Fe values tested from ICP are prominently promoted, which are even dozens of times that of the theoretical Na/Fe value of primary bulk xNa-FeO_x. It is speculated that there is a certain migration of Na from the iron-based catalyst to H-ZSM-5 after reaction. For more evidence, XPS results of spent H-ZSM-5 zeolites have been investigated, see Table 1. Na and Fe elements are detected on the surface of spent H-ZSM-5 catalysts. Notably, the mass contents of Fe measured by ICP and XPS are almost

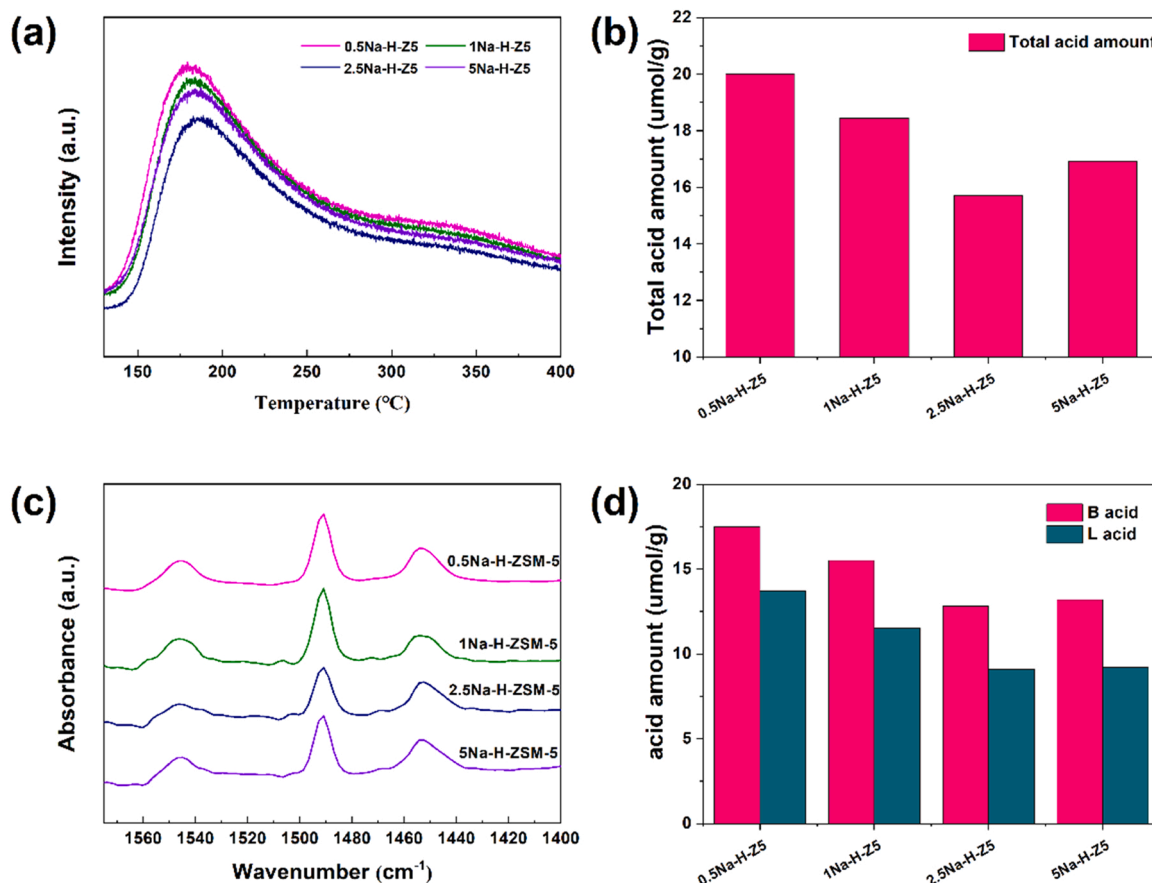


Fig. 4. (a) NH_3 -TPD and (c) Py-adsorption FTIR curves of fresh and spent H-ZSM-5 with different Na content loaded on Fe-based catalysts. (b), (d) The corresponding fitting data.

Table 1

The element content of spent $x\text{Na-H-ZSM-5}$ from ICP-OES and XPS measurement.

Samples	The content of Na/%		The content of Fe/%		Na/Fe		Na/Fe (Theoretical value)
	ICP	XPS	ICP	XPS	ICP	XPS	
0.5Na-H-ZSM-5	1.14	0.18	0.75	0.71	1.52	0.25	0.007
1Na-H-ZSM-5	1.17	0.25	0.73	0.70	1.61	0.36	0.014
2.5Na-H-ZSM-5	1.33	0.46	0.42	0.50	3.16	0.92	0.035
5Na-H-ZSM-5	1.28	0.38	0.36	0.37	3.55	1.03	0.070

unanimous, indicating that most of the iron is present on the surface of H-ZSM-5. Meanwhile, Na contents on the surface by XPS detection are lower than that from ICP measurements, albeit the Na/Fe ratios are still much higher than the corresponding theoretical values of primary bulk $x\text{Na-FeO}_x$, which proves a migration process of Na to H-ZSM-5 directly.

Further research is explored through TEM technique in combination with EDS for element composition analysis, see Fig. 5 and Table S5. As can be observed, the image of fresh H-ZSM-5 is not regular due to the hydrothermal treatment. However, the crystal structure remains intact as identified by XRD result. For EDS analysis, the main components are Si, Al, O, and P in the fresh H-ZSM-5 but without others. In the spent H-ZSM-5, 2.5Na-H-ZSM-5 being chosen typically (Fig. 5b, d and Table S5), a certain amount of Na element was detected. Fe element was not detected by EDS in the H-ZSM-5 fragments. These results also suggest that Na has migrated to H-ZSM-5, which affected the acidity and

eventually the reaction performance.

3.3. The necessity of Na migration for FTO-ZEO catalyst system

To clarify the necessity of Na migration process for improving the reaction performance of FTO-ZEO catalyst system, a control experiment has been devised. The catalytic performance of FTO-ZEO catalysts which contain H-ZSM-5 and a comparative H-ZSM-5 with Na doping were examined (see Fig. S3). Two kinds of Fe-based moiety with different Na contents, 0.5Na- FeO_x and 2.5Na- FeO_x , have been chosen to be combined with H-ZSM-5. The C_{5+} selectivity of 75.1 % over 2.5Na- FeO_x /H-ZSM-5 is better than the result of 67.9 % over 0.5Na- FeO_x /H-ZSM-5. As stated above, the difference can be attributed to the variation of Na contents in spent H-ZSM-5, showing a difference of 0.2Na as determined by ICP data. To further clarify the impact of sodium migration, a catalyst system by employing 0.2Na-im-H-ZSM-5 with direct impregnation of 0.2Na has been tested. It is shown that these tandem catalyst systems show comparable CO conversion. However, the tandem catalyst of 0.5Na- FeO_x /0.2Na-im-H-ZSM-5 shows much poor C_{5+} selectivity of 62.3 %. Therefore, the role of Na migration from $x\text{Na-FeO}_x$ to H-ZSM-5 during FT reaction cannot be simply replaced by impregnation of Na on H-ZSM-5.

3.4. Reaction paths of FTO-ZEO catalyst system modified by Na

In the above section, the way that Na affects zeolites with a migration behavior has been clarified. However, the way that how do Na promotor affect the properties of zeolites and more importantly the F-T synthesis performance deserves further research. The liquid products collected by cold trap have been analyzed by GC-MS (see Fig. S4). The products from $x\text{Na-FeO}_x$ catalysts are mainly olefins and alkanes (Fig. S4A and B).

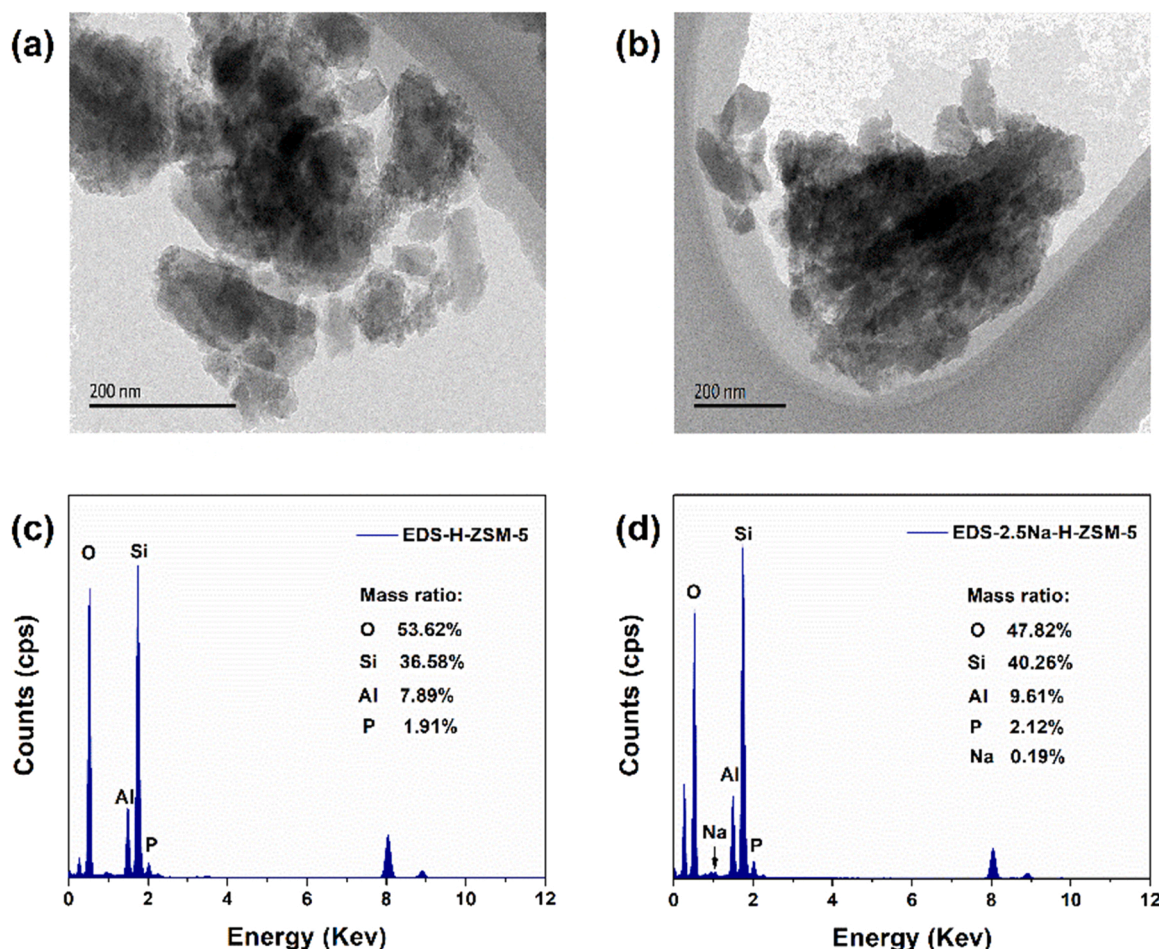


Fig. 5. (a), (c) TEM images and (b), (d) EDS results of fresh H-ZSM-5 and spent 2.5Na-H-ZSM-5.

While, the products from xNa-FeO_x and H-ZSM-5 tandem catalysts are mainly aromatics and alkanes (Fig. S4C and D). This phenomenon suggests that the introduction of zeolite transforms olefins into aromatics and alkanes, making the chemical equilibrium move forward and the products transform into high carbon products.

Based on qualitative analysis of GC-MS results, full composition analysis of hydrocarbon products has been obtained (Fig. 6). For iron-based catalysts within the platform period, the 0.5Na-FeO_x and 2.5Na-FeO_x catalysts show similar product selectivities. After calculation and data fitting, the product distribution of the two catalysts conforms to the ASF distribution with the chain growth probability (α value) of 0.65. The similar distribution in different carbon numbers further confirms that there is slight change in catalytic performance during the platform period. Comparatively, the tandem catalyst systems exhibit obvious variations in product distribution. For 0.5Na-FeO_x and H-ZSM-5, the selectivity of olefin is decreased

while that of aromatics increases (Fig. 6c). The product selectivity deviates from the linear correlation with ASF distribution, with the α value increases from 0.65 to 0.78. Furthermore, with the increase of Na content, the reaction tends to produce more products with higher carbon, especially aromatics (Fig. 6d). As determined, the highest carbon number of products are 12, which suggests nearly all of C₅₊ products are in the gasoline range. Therefore, under optimal reaction conditions, about 72 % of gasoline product can be obtained by Na modified FTO-ZEO system.

In order to clarify why Na promotor may affect the product distribution of FTO-ZEO system, model experiments of ethylene conversion were carried out. For such tandem catalysts, olefins are generally considered to be intermediates in obtaining high carbon products from

syngas. Zeolites affect the distribution of the final product directly. Therefore, ethylene is used as a model of feed to investigate the catalytic performance of spent H-ZSM-5 (Table S6). As shown in Fig. 7, the transformation of C₂H₄ and a gas mixture of C₂H₄ and H₂ on spent xNa-H-ZSM-5 has been examined. For the spent H-ZSM-5 with more Na promotor (2.5Na-HZSM-5), the conversion degree of C₂H₄ and mixed gas are both low. In combination with the above discussions, the migration of Na affects the acidity of H-ZSM-5 and reduces its ability of olefins conversion. In presence of H₂, the conversion of ethylene (ethylene hydrogenation) reduces much faster than the situation without H₂ (ethylene polymerization). Thus, the migration of Na inhibits the hydrogenation of olefin on H-ZSM-5 obviously, leading to produce higher carbon products. Focusing on product selectivity, the catalysts reacted in the mixture of C₂H₄ and H₂ produce a large amount of low-carbon alkanes on zeolites. However, the main products of ethylene on spent H-ZSM-5 are aromatics and high-carbon alkanes. Combined with the former results

of full-component analysis, it is further proved that the migration of Na into zeolites inhibits the olefin hydrogenation ability, promoting the selectivity toward high carbon products in the FTO-ZEO system.

Based on the above discussion, the reaction path of syngas on the Na-modified FTO-ZEO system has been inferred and displayed in Fig. 8. Firstly, the syngas reacted to form olefins on the Na modified iron-based catalyst. Meanwhile, there is a migration process of Na from FeO_x to the H-ZSM-5, which affects the acidity of zeolites and suppresses the hydrogenation of olefins. As the olefin intermediates enter into the zeolites, the products move toward high carbon components and mainly rank in the range of gasoline.

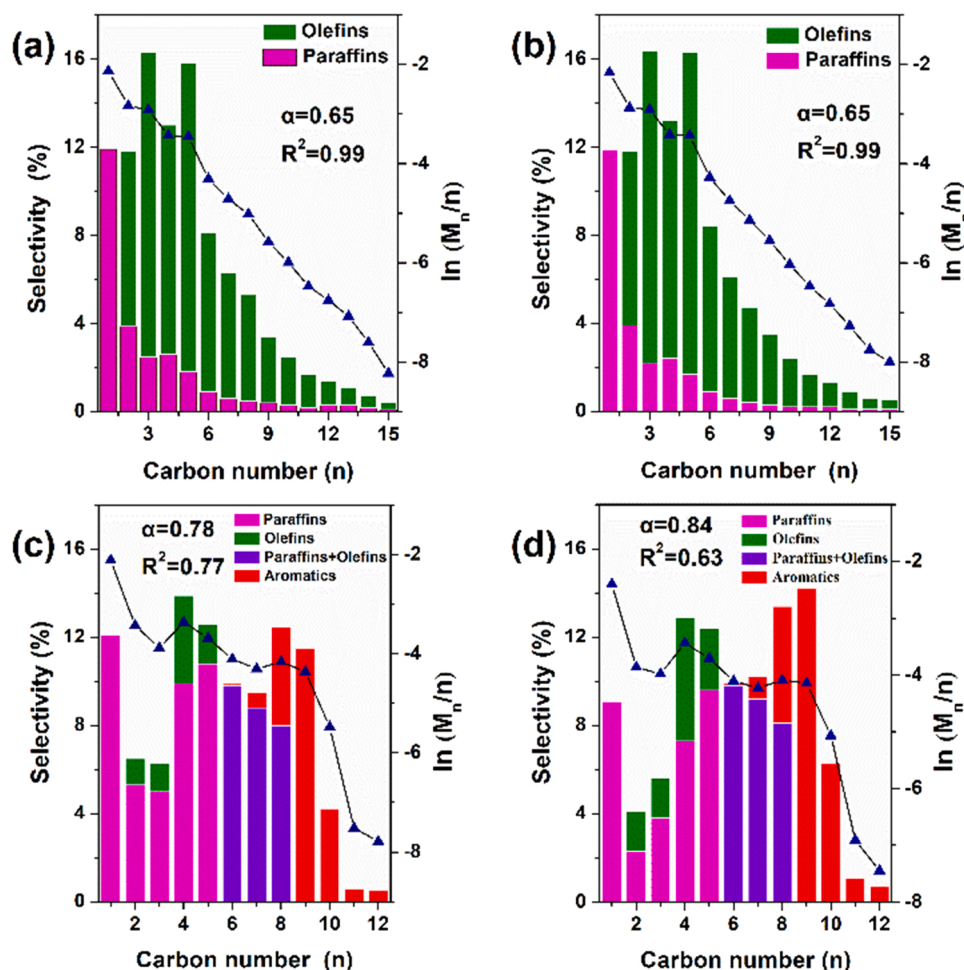


Fig. 6. ASF plots of product distribution over (a) 0.5Na-FeO_x, (b) 2.5Na-FeO_x, (c) 0.5Na-FeO_x and H-ZSM-5, (d) 2.5Na-FeO_x and H-ZSM-5 catalysts. The calculated chain growth probability (α value) and the weight fraction (W_n , the selectivity) of products with their carbon atoms have also been given.

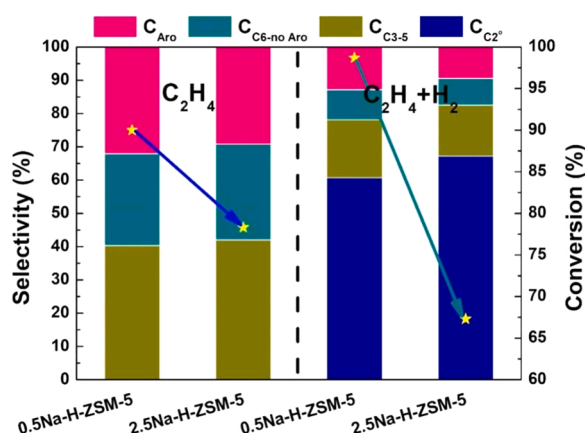


Fig. 7. The reaction performance of ethylene conversion model experiments over spent xNa-H-ZSM-5 catalysts. Reaction conditions: 200 mg spent xNa-H-ZSM-5, 320 °C, 3 MPa, 6000 ml g_{cat}⁻¹ h⁻¹, C₂H₄/Ar = 15/85 and C₂H₄/H₂/Ar = 15/15/70.

4. Conclusion

In this work, xNa-FeO_x and H-ZSM-5 tandem catalysts are adopted to construct the FTO-ZEO catalyst system. The influence of Na in this system has been investigated by varying the content of Na on the iron-based catalyst. Compared with bare FeO_x catalysts, which perform a

performance-platform period (0.5–5 %Na), the tandem catalysts show high syngas conversion and high selectivity toward gasoline product. The effect of Na on iron-based catalysts and on the physical properties of H-ZSM-5 have been excluded by a set of characterizations. With further exploration, a migration process of Na to the H-ZSM-5 has been identified as the key factor that affects the acidity and eventually the reaction performance. By conducting ethylene conversion model experiments, it is verified that the migration of Na shows great hindrance of C₂H₄ hydrogenation on zeolites, which renders the products moving toward gasoline constituents. The present work explores the influence of Na promoter on the two active moieties in the FTO-ZEO system. It paves us a better way to understand the tandem catalyst system and zeolite modification during the reaction processes.

CRediT authorship contribution statement

Ruifeng Wang: Investigation, Formal analysis, Visualization, Writing – original draft, Writing – review & editing. **Binglian Liang:** Investigation, Writing – review & editing. **Xiaoli Yang:** Formal analysis. **Xuning Li:** Formal analysis, Writing – review & editing. **Yaru Zhang:** Formal analysis. **Guodong Liu:** Formal analysis. **Xiong Su:** Conceptualization, Methodology, Supervision, Writing – review & editing. **Yan-qiang Huang:** Conceptualization, Methodology, Supervision. **Tao Zhang:** Methodology, Supervision.

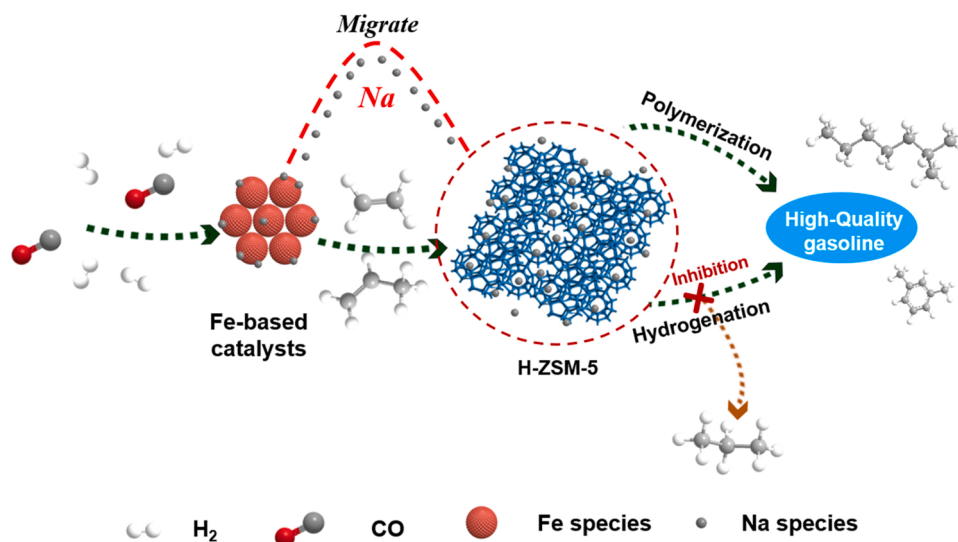


Fig. 8. Scheme of the migration and feasible role of sodium in iron-based FT-Zeolite composite catalyst system for syngas conversion.

Declaration of Competing Interest

The authors declare that they have no known competing financial interests or personal relationships that could have appeared to influence the work reported in this paper.

Data Availability

Data will be made available on request.

Acknowledgment

The authors gratefully acknowledge the Strategic Priority Research Program of the Chinese Academy of Sciences (No. XDA29040600 and No. XDB36030200), the National Natural Science Foundation of China (21978286, 21925803), the Youth Innovation Promotion Association CAS, the Young Top-notch Talents of Liaoning Province (XLYC2007082), and the China Scholarship Council (2020M670807).

Appendix A. Supporting information

Supplementary data associated with this article can be found in the online version at [doi:10.1016/j.apcatb.2022.122132](https://doi.org/10.1016/j.apcatb.2022.122132).

References

- [1] W. Zhou, K. Cheng, J. Kang, C. Zhou, V. Subramanian, Q. Zhang, Y. Wang, New horizon in C_1 chemistry: breaking the selectivity limitation in transformation of syngas and hydrogenation of CO_2 into hydrocarbon chemicals and fuels, *Chem. Soc. Rev.* 48 (2019) 3193–3228, <https://doi.org/10.1039/c8cs00502h>.
- [2] J. Li, Y. He, L. Tan, P. Zhang, X. Peng, A. Oruganti, G. Yang, H. Abe, Y. Wang, N. Tsubaki, Integrated tuneable synthesis of liquid fuels via Fischer-Tropsch technology, *Nat. Catal.* 1 (2018) 787–793, <https://doi.org/10.1038/s41929-018-0144-z>.
- [3] S. Liu, A.C. Gujar, P. Thomas, H. Toghiani, M.G. White, Synthesis of gasoline-range hydrocarbons over Mo/HZSM-5 catalysts, *Appl. Catal. A* 357 (2009) 18–25, <https://doi.org/10.1016/j.apcata.2008.12.033>.
- [4] X. Wang, C. Zeng, N. Gong, T. Zhang, Y. Wu, J. Zhang, F. Song, G. Yang, Y. Tan, Effective suppression of CO selectivity for CO_2 hydrogenation to high-quality gasoline, *ACS Catal.* 11 (2021) 1528–1547, <https://doi.org/10.1021/acscatal.0c04155>.
- [5] P. Wang, W. Chen, F.-K. Chiang, A.I. Dugulan, Y. Song, R. Pestman, K. Zhang, J. Yao, B. Feng, P. Miao, W. Xu, E.J.M. Hensen, Synthesis of stable and low- CO_2 selective ϵ -iron carbide Fischer-Tropsch catalysts, *Sci. Adv.* 4 (2018) eaau2947, <https://doi.org/10.1126/sciadv.aau2947>.
- [6] H.M. Torres Galvis, J.H. Bitter, C.B. Khare, M. Ruitenbeek, A.I. Dugulan, K.P. de Jong, Supported iron nanoparticles as catalysts for sustainable production of lower olefins, *Science* 335 (2012) 835–838, <https://doi.org/10.1126/science.1215614>.
- [7] P. Zhai, C. Xu, R. Gao, X. Liu, M. Li, W. Li, X. Fu, C. Jia, J. Xie, M. Zhao, X. Wang, Y. W. Li, Q. Zhang, X.D. Wen, D. Ma, Highly tunable selectivity for syngas-derived alkenes over zinc and sodium-modulated Fe_3C_2 catalyst, *Angew. Chem. Int. Ed.* 55 (2016) 9902–9907, <https://doi.org/10.1002/anie.201603556>.
- [8] X. Yang, R. Wang, J. Yang, W. Qian, Y. Zhang, X. Li, Y. Huang, T. Zhang, D. Chen, Exploring the reaction paths in the consecutive Fe-based FT catalyst-zeolite process for syngas conversion, *ACS Catal.* 10 (2020) 3797–3806, <https://doi.org/10.1021/acscatal.9b05449>.
- [9] Y. Piao, Q. Jiang, H. Li, H. Matsumoto, J. Liang, W. Liu, C. Pham-Huu, Y. Liu, F. Wang, Identify Zr promotion effects in atomic scale for Co-based catalysts in Fischer-Tropsch synthesis, *ACS Catal.* 10 (2020) 7894–7906, <https://doi.org/10.1021/acscatal.0c01874>.
- [10] Y. Zhang, X. Yang, X. Yang, H. Duan, H. Qi, Y. Su, B. Liang, H. Tao, B. Liu, X. Chen, Y. Su, T. Huang, Zhang, Tuning reactivity of Fischer-Tropsch synthesis by regulating TiO_x overlayer over Ru/ TiO_2 nanocatalysts, *Nat. Commun.* 11 (2020) 3185, <https://doi.org/10.1038/s41467-020-17044-4>.
- [11] M.E. Dry, The Fischer-Tropsch process: 1950–2000, *Catal. Today* 71 (2002) 227–241, [https://doi.org/10.1016/S0920-5861\(01\)00453-9](https://doi.org/10.1016/S0920-5861(01)00453-9).
- [12] L. Tang, L. He, Y. Wang, B. Chen, W. Xu, X. Duan, A.-H. Lu, Selective fabrication of χ - Fe_5C_2 by interfering surface reactions as a highly efficient and stable Fischer-Tropsch synthesis catalyst, *Appl. Catal. B* 284 (2021), <https://doi.org/10.1016/j.apcatb.2020.119753>.
- [13] B. Liu, W. Li, J. Zheng, Q. Lin, X. Zhang, J. Zhang, F. Jiang, Y. Xu, X. Liu, CO_2 formation mechanism in Fischer-Tropsch synthesis over iron-based catalysts: a combined experimental and theoretical study, *Catal. Sci. Technol.* 8 (2018) 5288–5301, <https://doi.org/10.1039/c8cy01621f>.
- [14] R.A. Friedel, R.B. Anderson, Composition of synthetic liquid fuels product distribution and analysis of C_5 – C_8 paraffin isomers from cobalt catalyst, *J. Am. Chem. Soc.* 72 (1950) 1212–1215, <https://doi.org/10.1021/ja01159a039>.
- [15] R.L. Varma, N.N. Bakhshi, J.F. Mathews, S.H. Ng, Performance of dual-reactor system for conversion of syngas to aromatic-containing hydrocarbons, *Ind. Eng. Chem. Res.* 26 (1987) 183–188, <https://doi.org/10.1021/ie00062a001>.
- [16] F. Jiao, J. Li, X. Pan, J. Xiao, H. Li, H. Ma, M. Wei, Y. Pan, Z. Zhou, M. Li, S. Miao, J. Li, Y. Zhu, D. Xiao, T. He, J. Yang, F. Qi, Q. Fu, X. Bao, Selective conversion of syngas to light olefins, *Science* 351 (2016) 1065–1068, <https://doi.org/10.1126/science.aaf1835>.
- [17] N. Li, F. Jiao, X. Pan, Y. Chen, J. Feng, G. Li, X. Bao, High-quality gasoline directly from syngas by dual metal oxide-zeolite (OX-ZEO) catalysis, *Angew. Chem. Int. Ed.* 58 (2019) 7400–7404, <https://doi.org/10.1002/anie.201902990>.
- [18] B. Zhao, P. Zhai, P. Wang, J. Li, T. Li, M. Peng, M. Zhao, G. Hu, Y. Yang, Y.-W. Li, Q. Zhang, W. Fan, D. Ma, Direct transformation of syngas to aromatics over Na-Zn- Fe_5C_2 and hierarchical HZSM-5 tandem catalysts, *Chem* 3 (2017) 323–333, <https://doi.org/10.1016/j.chempr.2017.06.017>.
- [19] Y. Xu, J. Wang, G. Ma, J. Zhang, M. Ding, Hollow zeolite nanoparticles combined with $Fe_3O_4@MnO_2$ tandem catalyst for converting syngas to aromatics-rich gasoline, *ACS Appl. Nano Mater.* 3 (2020) 2857–2866, <https://doi.org/10.1021/acsnano.0c00123>.
- [20] J.L. Weber, I. Dugulan, P.E. deJongh, K.P. deJong, Bifunctional catalysis for the conversion of synthesis gas to olefins and aromatics, *ChemCatChem* 10 (2018) 1107–1112, <https://doi.org/10.1002/cctc.201701667>.
- [21] Y. Xu, D. Liu, X. Liu, Conversion of syngas toward aromatics over hybrid Fe-based Fischer-Tropsch catalysts and HZSM-5 zeolites, *Appl. Catal. A* 552 (2018) 168–183, <https://doi.org/10.1016/j.apcata.2018.01.012>.
- [22] Y. Xu, J. Wang, G. Ma, J. Bai, Y. Du, M. Ding, Direct synthesis of aromatics from syngas over Mo-modified Fe/HZSM-5 bifunctional catalyst, *Appl. Catal. A* 598 (2020), 117589, <https://doi.org/10.1016/j.apcata.2020.117589>.

- [23] Y. Xu, J. Liu, G. Ma, J. Wang, J. Lin, H. Wang, C. Zhang, M. Ding, Effect of iron loading on acidity and performance of Fe/HZSM-5 catalyst for direct synthesis of aromatics from syngas, *Fuel* 228 (2018) 1–9, <https://doi.org/10.1016/j.fuel.2018.04.151>.
- [24] J. Plana-Pallejà, S. Abelló, C. Berrueto, D. Montané, Effect of zeolite acidity and mesoporosity on the activity of Fischer–Tropsch Fe/ZSM-5 bifunctional catalysts, *Appl. Catal. A* 515 (2016) 126–135, <https://doi.org/10.1016/j.apcata.2016.02.004>.
- [25] Y. Xu, J. Liu, J. Wang, G. Ma, J. Lin, Y. Yang, Y. Li, C. Zhang, M. Ding, Selective conversion of syngas to aromatics over $\text{Fe}_3\text{O}_4/\text{MnO}_2$ and hollow HZSM-5 bifunctional catalysts, *ACS Catal.* 9 (2019) 5147–5156, <https://doi.org/10.1021/acscatal.9b01045>.
- [26] A.J. Barrios, B. Gu, Y. Luo, D.V. Peron, P.A. Chernavskii, M. Virginie, R. Wojcieszak, J.W. Thybaut, V.V. Ordonsky, A.Y. Khodakov, Identification of efficient promoters and selectivity trends in high temperature Fischer–Tropsch synthesis over supported iron catalysts, *Appl. Catal. B* 273 (2020), 119028, <https://doi.org/10.1016/j.apcatb.2020.119028>.
- [27] J. Li, X. Cheng, C. Zhang, Q. Chang, J. Wang, X. Wang, Z. Lv, W. Dong, Y. Yang, Y. Li, Effect of alkalis on iron-based Fischer–Tropsch synthesis catalysts: alkali- FeO_x interaction, reduction, and catalytic performance, *Appl. Catal. A* 528 (2016) 131–141, <https://doi.org/10.1016/j.apcata.2016.10.006>.
- [28] J. Wei, Q. Ge, R. Yao, Z. Wen, C. Fang, L. Guo, H. Xu, J. Sun, Directly converting CO_2 into a gasoline fuel, *Nat. Commun.* 8 (2017) 15174, <https://doi.org/10.1038/ncomms15174>.
- [29] G. Ma, Y. Xu, J. Wang, J. Bai, Y. Du, J. Zhang, M. Ding, An Na-modified Fe@C core-shell catalyst for the enhanced production of gasoline-range hydrocarbons via Fischer–Tropsch synthesis, *Rsc Adv.* 10 (2020) 10723–10730, <https://doi.org/10.1039/d0ra01036g>.
- [30] H. Xiong, M.A. Motchelaho, M. Moyo, L.L. Jewell, N.J. Coville, Effect of group I alkali metal promoters on Fe/CNT catalysts in Fischer–Tropsch synthesis, *Fuel* 150 (2015) 687–696, <https://doi.org/10.1016/j.fuel.2015.02.099>.
- [31] J. Li, X. Cheng, C. Zhang, Y. Yang, Y. Li, Effects of alkali on iron-based catalysts for Fischer–Tropsch synthesis: CO chemisorptions study, *J. Mol. Catal. A* 396 (2015) 174–180, <https://doi.org/10.1016/j.molcata.2014.10.006>.
- [32] J. Wei, J. Sun, Z. Wen, C. Fang, Q. Ge, H. Xu, New insights into the effect of sodium on Fe_3O_4 -based nanocatalysts for CO_2 hydrogenation to light olefins, *Catal. Sci. Technol.* 6 (2016) 4786–4793, <https://doi.org/10.1039/c6cy00160b>.
- [33] Y. Wang, G. Wang, L.I. van der Wal, K. Cheng, Q. Zhang, K.P. de Jong, Y. Wang, Visualizing element migration over bifunctional metal-zeolite catalysts and its impact on catalysis, *Angew. Chem. Int. Ed.* 60 (2021) 17735–17743, <https://doi.org/10.1002/anie.202107264>.
- [34] T. Wang, Y. Xu, Y. Li, L. Xin, B. Liu, F. Jiang, X. Liu, Sodium-mediated bimetallic Fe–Ni catalyst boosts stable and selective production of light aromatics over HZSM-5 zeolite, *ACS Catal.* 11 (2021) 3553–3574, <https://doi.org/10.1021/acscatal.1c00169>.
- [35] M. Li, M.A. Nawaz, G. Song, W.Q. Zaman, D. Liu, Influential role of elemental migration in a composite iron–zeolite catalyst for the synthesis of aromatics from syngas, *Ind. Eng. Chem. Res.* 59 (2020) 9043–9054, <https://doi.org/10.1021/acs.iecr.0c01282>.
- [36] B. Liang, H. Duan, T. Sun, J. Ma, X. Liu, J. Xu, X. Su, Y. Huang, T. Zhang, Effect of Na promoter on Fe-based catalyst for CO_2 hydrogenation to alkenes, *ACS Sustain. Chem. Eng.* 7 (2018) 925–932, <https://doi.org/10.1021/acssuschemeng.8b04538>.
- [37] W. Ngantsoue-Hoc, Y. Zhang, R.J. O'Brien, M. Luo, B.H. Davis, Fischer–Tropsch synthesis: activity and selectivity for Group I alkali promoted iron-based catalysts, *Appl. Catal. A* 236 (2002) 77–89, [https://doi.org/10.1016/S0926-860X\(02\)00278-8](https://doi.org/10.1016/S0926-860X(02)00278-8).
- [38] M. Ding, Y. Yang, B. Wu, Y. Li, T. Wang, L. Ma, Study on reduction and carburization behaviors of iron phases for iron-based Fischer–Tropsch synthesis catalyst, *Appl. Energy* 160 (2015) 982–989, <https://doi.org/10.1016/j.apenergy.2014.12.042>.
- [39] M. Ding, Y. Yang, J. Xu, Z. Tao, H. Wang, H. Wang, H. Xiang, Y. Li, Effect of reduction pressure on precipitated potassium promoted iron–manganese catalyst for Fischer–Tropsch synthesis, *Appl. Catal. A* 345 (2008) 176–184, <https://doi.org/10.1016/j.apcata.2008.04.036>.
- [40] Y. Liu, J.-F. Chen, J. Bao, Y. Zhang, Manganese-modified Fe_3O_4 microsphere catalyst with effective active phase of forming light olefins from syngas, *ACS Catal.* 5 (2015) 3905–3909, <https://doi.org/10.1021/acscatal.5b00492>.
- [41] X.W. Liu, S. Zhao, Y. Meng, Q. Peng, A.K. Dearden, C.F. Huo, Y. Yang, Y.W. Li, X. D. Wen, Mossbauer spectroscopy of iron carbides: from prediction to experimental confirmation, *Sci. Rep.* 6 (2016) 26184, <https://doi.org/10.1038/srep26184>.
- [42] E.P. Sajitha, V. Prasad, S.V. Subramanyam, A.K. Mishra, S. Sarkar, C. Bansal, Size-dependent magnetic properties of iron carbide nanoparticles embedded in a carbon matrix, *J. Phys.: Condens. Matter* 19 (2007), 046214, <https://doi.org/10.1088/0953-8984/19/4/046214>.
- [43] R. Miyatani, Y. Yamada, Y. Kobayashi, Mössbauer study of iron carbide nanoparticles produced by sonochemical synthesis, *J. Radioanal. Nucl. Chem.* 303 (2014) 1503–1506, <https://doi.org/10.1007/s10967-014-3507-1>.
- [44] B. Kniep, A. Constantinescu, D. Niemeier, K.D. Becker, Anin-situ Mössbauer study of the formation of cementite, Fe_3C , *Z. Anorg. Allg. Chem.* 629 (2003) 1795–1804, <https://doi.org/10.1002/zaac.200300136>.